5424 *Inorg. Chem.* **2010**, *49*, 5424–5431
DOI: 10.1021/ic902430w

Inorganic Chemistry
Article

Solution Synthesis and Characterization of Indium−Zinc Formate Precursors for Transparent Conducting Oxides

Robert M. Pasquarelli,*,† Calvin J. Curtis,‡ Alexander Miedaner,‡ Maikel F.A.M. van Hest,‡ Ryan P. O'Hayre,† and David S. Ginley‡

†*Colorado School of Mines, Metallurgical and Materials Engineering, 1500 Illinois Street, Golden, Colorado 80401, and* ‡*National Renewable Energy Laboratory, 1617 Cole Boulevard, Golden, Colorado 80401*

Received December 7, 2009

A series of In−Zn formate mixtures were investigated as potential precursors to amorphous In−Zn-oxide (IZO) for transparent conducting oxide (TCO) applications. These mixtures were prepared by neutralization from formic acid and characterized by elemental analysis, IR spectroscopy, powder X-ray diffraction, and thermogravimetry-differential scanning calorimetry (TG-DSC) measurements. Thermal analysis revealed that a mixture of In and Zn formates reduced the overall decomposition temperature compared to the individual constituents and that OH-substitution enhanced the effect. In terms of precursor feasibility, it was demonstrated that the decomposition products of In−Zn formate could be directed toward oxidation or reduction by controlling the decomposition atmosphere or with solution acid additives. For TCO applications, amorphous IZO films were prepared by ultrasonic spray deposition from In−Zn formate solutions with annealing at 300−400 °C.

Introduction

Transparent conducting oxide (TCO) thin films play a critical role in many current and emerging opto-electronic devices. Their unique combination of high transparency in the visible region of the spectrum and tunable electronic conductivity is ideal for applications in displays, transparent thin-film transistors (TTFTs), and solar cells.[1−3] TCO composition-space is composed of mixed binary and ternary oxides of Sn, In, Zn, Ga, and Al.[4−8] Solution deposition routes to these metal oxides employ chemical precursors, typically in the form of acetates, chlorides, nitrates, or acetylacetonates.[9−19] Precursors for In and Zn are of particular interest as many now consider amorphous In−Zn-oxide (a-IZO) to be the archetype amorphous oxide semiconductor material.[6−8,20]

While examples of the use of acetate precursors are numerous,[9−16] the use of formate precursors for TCOs is rare.[21] Here we investigate the synthesis and properties of the formates of In and Zn as potential IZO precursors. Formate is the simplest carboxylate form, thus having the smallest steric effect. It can bind to metal cations in various ways as mono- or polydentate ligands. The formates of divalent 3d transition metals (M = Zn, Mg, Cu, Mn, Ni, Cd)[22−29] are

*To whom correspondence should be addressed. E-mail: robert.pasquarelli@nrel.gov.

(1) Lewis, B. G.; Paine, D. C. *MRS Bull.* **2000**, *25*, 22.
(2) Ginley, D. S.; Bright, C. *MRS Bull.* **2000**, *25*, 15.
(3) Fortunato, E.; Ginley, D. S.; Hosono, H.; Paine, D. C. *MRS Bull.* **2007**, *32*, 242.
(4) Minami, T. *MRS Bull.* **2000**, *25*, 38.
(5) Coutts, T. J.; Young, D. L.; Li, X. *MRS Bull.* **2000**, *25*, 58.
(6) Taylor, M. P.; Readey, D. W.; Teplin, C. W.; van Hest, M. F. A. M.; Alleman, J. L.; Dabney, M. S.; Gedvilas, L. M.; Keyes, B. M.; To, B.; Perkins, J. D.; Ginley, D. S. *Meas. Sci. Technol.* **2005**, *16*, 90.
(7) Taylor, M. P.; Readey, D. W.; van Hest, M. F. A. M.; Teplin, C. W.; Alleman, J. L.; Dabney, M. S.; Gedvilas, L. M.; Keyes, B. M.; To, B.; Perkins, J. D.; Ginley, D. S. *Adv. Funct. Mater.* **2008**, *18*(20), 3169.
(8) Perkins, J. D.; van Hest, M. F. A. M.; Taylor, M. P.; Ginley, D. S. *Int. J. Nanotechnol.* **2009**, *6*(9), 850.
(9) Jin-Hong, L.; Byung-Ok, P. *Thin Solid Films* **2003**, *426*, 94.
(10) Chang-Hyun, K.; Jin-Hong, L.; Byung-Ok, P. *Mater. Sci. Forum* **2004**, *449−452*, 469.
(11) Seung-Yup, L.; Byung-Ok, P. *Thin Solid Films* **2005**, *484*, 184.
(12) de la Luz Olvera, M.; Gomez, H.; Maldonado, A. *Sol. Energy Mater. Sol. Cells* **2007**, *91*, 1449.
(13) Choi, C. G.; Seo, S.-J.; Bae, B.-S. *Electrochem. Solid-State Lett.* **2008**, *11*, H7.
(14) Wienke, J.; Booij, A. S. *Thin Solid Films* **2008**, *516*, 4508.
(15) Wienke, J.; van der Zanden, B.; Tijssen, M.; Zeman, M. *Sol. Energy Mater. Sol. Cells* **2008**, *92*, 884.
(16) Kim, G. H.; Shin, H. S.; Ahn, B. D.; Kim, K. H.; Park, W. J.; Kim, H. J. *J. Electrochem. Soc.* **2009**, *156*, H7.
(17) Agashe, C.; Hupkes, J.; Schope, G.; Berginski, M. *Sol. Energy Mater. Sol. Cells* **2009**, *93*, 1256.
(18) Maldonado, A.; de la Luz Olvera, M.; Tirado Guerrab, S.; Asomozaa, R. *Sol. Energy Mater. Sol. Cells* **2004**, *82*, 75.
(19) Moses Ezhil Raja, A.; Lalithambikab, K. C.; Vidhyac, V. S.; Rajagopalc, G.; Thayumanavand, A.; Jayachandranc, M.; Sanjeevirajae, C. *Physica B* **2008**, *403*, 544.
(20) Hosono, H. *J. Non-Cryst. Solids* **2006**, *352*, 851.
(21) Seki, S.; Sawada, Y.; Ogawa, M.; Yamamoto, M.; Kagota, Y.; Shida, A.; Ide, M. *Surf. Coat. Technol.* **2003**, *167−170*, 525.
(22) Osaki, K.; Nakai, Y.; Watanabé, T. *J. Phys. Soc. Jpn.* **1963**, *18*, 919.
(23) Burger, V. N.; Fuess, H. *Z. Kristallogr.* **1977**, *145*, 346.
(24) de With, G.; Harkema, S.; van Hummel, G. J. *Acta Crystallogr.* **1976**, *B32*, 1980.
(25) Bukowska-Strzyzewska, M. *Acta Crystallogr.* **1965**, *19*, 357.
(26) Radhakrishna, P.; Gillon, B.; Chevrier, G. *J. Phys.: Condens. Matter* **1993**, *5*(35), 6447.

Published on Web 05/24/2010

well-known and form isostructural-monoclinic crystals with the general formula $M(HCOO)_2 \cdot 2H_2O$. In their dihydrate form, the formate ions bind μ_2. Conversely, in their anhydrous form $M(HCOO)_2$ (M = Zn, Mg, Cu, Mn),[30−33] the formate ions coordinate μ_3. $Zn(HCOO)_2 \cdot 2H_2O$ has been synthesized by neutralizing the oxide[34] and hydroxide carbonate[35] with formic acid. Trivalent metal formates have been studied less extensively than divalent metal formates. The indium formates consist of InO_6 octahedra and exhibit various formate and hydroxyl bridging modes. $In(HCOO)_3$ (hexagonal), $In_2(HCOO)_5(OH)$ (monoclinic), and $In(HCOO)_2(OH)$ (tetragonal) have been produced by hydrothermal synthesis.[36] $In(HCOO)_3$ has also been made by neutralization of the oxide.[21]

In this article, we report on the characterization of a series of co-synthesized In−Zn formate mixtures exhibiting various degrees of hydration and OH-substitution prepared by neutralization from formic acid: $Zn(HCOO)_2 \cdot 2H_2O$ + hexagonal $In(HCOO)_2(OH)$, anhydrous $Zn(HCOO)_2$ + hexagonal $In(HCOO)_3$, and $Zn(HCOO)_2 \cdot 2H_2O$ + tetragonal $In(HCOO)_2(OH)$ with compositions ranging 70−86 cation% In. Thermal analysis revealed that a mixture of In and Zn formates reduced the overall decomposition temperature compared to the individual constituents and that OH-substitution enhanced the effect. As a precursor, it was demonstrated that the decomposition products of In−Zn formate could be directed toward oxidation or reduction by controlling the decomposition atmosphere or with solution additives such as acids. Additionally, as demonstration for TCO applications, amorphous IZO films were solution deposited using In−Zn formates.

Experimental Section

Materials and Instrumentation. Zinc hydroxide carbonate $[ZnCO_3]_2 \cdot [Zn(OH)_2]_3$ and In_2O_3 were obtained from Riedel-de Haën and Materials Research Corporation, respectively. Formic acid (HCOOH) and solvents were from Sigma-Aldrich. Starting materials were used as supplied without further purification.

Infrared spectroscopy was performed on a Nicolet Nexus 870 FTIR spectrometer equipped with a Pike Technologies MIRacle diamond ATR at 2 cm^{-1} resolution. To determine the decomposition behavior, simultaneous thermogravimetry (TG) and differential scanning calorimetry (DSC) were performed under dry air and N_2 atmospheres in alumina pans with a heating rate of 10 °C/min using a TA Instruments SDT Q600 analyzer. Precursor metal ratios were determined by inductively coupled plasma atomic emission spectroscopy (ICP-AES) and confirmed by X-ray fluorescence (XRF). ICP-AES solutions in 5% HNO_3−deionized water were analyzed on a Varian Liberty 150 spectrometer. XRF measurements were performed on a Matrix Metrologies MaXXi 5 with W anode, 800-μm collimator, and 30 s scan time. Elemental analysis of carbon and hydrogen was performed by Huffman Laboratories Inc. (Golden, CO) with a combustion microanalyzer with coulometric detection. A Bruker AXS D8 Discover X-ray diffraction (XRD) system with a Cu Kα radiation source and large area GADDS detector was used for structural analysis. The calculated molecular formulas of the products are based on a combination of metals, C−H, IR, and thermogravimetric analyses.

Precursor solutions consisted of 0.1 M In−Zn formate (**3a**) in a methanol−water−acid (6:1:0.2 vol) mixture. HCOOH and conc. HNO_3 were used as acid additives. Drop-casting was performed onto microscope glass at 300 °C in air. Films were deposited using a custom ultrasonic spray system consisting of a Sono-Tek Model 8700 spray head driven at 120 kHz, a N_2 fed directional nozzle, a Fluid Metering Inc. VMP TRI pump, and a heated platen mounted on X-Y slide stages. Films were annealed in a Lindberg Model 59344 tube furnace with a 3 h ramp and 20 min hold at 300−400 °C under Ar-4%H_2.

Synthesis of $Zn(HCOO)_2 \cdot 2H_2O$ (1). HCOOH (0.66 mol, 25 mL) was added with stirring to zinc hydroxide carbonate (7.36 mmol, 4.04 g) in a 50 mL round-bottom flask fitted with a condenser vented to atmosphere. The mixture bubbled upon addition, and a white suspension resulted. The mixture was heated at 80 °C in an oil bath for 5 h. After cooling to room temperature, the precipitate was collected via suction filtration, washed with tetrahydrofuran (THF), and then dried under aspiration to remove residual formic acid. Small white crystals were obtained (3.26 g, 59% yield). IR spectrum (cm^{-1}): 3346m, 3268m, 3170m, 2984vw, 2900w, 1667w, 1560vs, 1396m, 1374s, 1352vs, 878w, 836w, 761m, 722m, and 565m. Anal. Calcd for $Zn(HCOO)_2 \cdot 2H_2O$ (FW 191.47): C 12.55, H 3.16. Found: C 12.60, H 3.26.

Synthesis of $In(HCOO)_3$ (2). HCOOH (0.66 mol, 25 mL) was added with stirring to In_2O_3 (10.9 mmol, 3.04 g) in a 50 mL round-bottom flask fitted with a condenser. The mixture was heated at 80 °C in an oil bath for 2 weeks, over which the suspension gradually whitened in appearance. The product was collected and washed in the same way as **1**. A white powder with yellow tint was obtained (5.45 g, 99% yield). IR spectrum (cm^{-1}): 2986vw, 2913w, 1633m, 1572s, 1543vs, 1402m, 1387s, 1363vs, and 792vs. Anal. Calcd for $In(HCOO)_3$ (FW 249.87): C 14.42, H 1.21. Found: C 14.08, H 1.21.

Synthesis of $In_xZn_{(1-x)}(HCOO)_{(2+x-y)}(OH)_y \cdot zH_2O$ (3). Prepared with a starting In:Zn of 65:35 at % (**3a**). HCOOH (0.80 mol, 30 mL) was added with rapid stirring to fine mixture of In_2O_3 (13.0 mmol, 3.61 g, 26 mmol In) and zinc hydroxide carbonate (2.81 mmol, 1.54 g, 14 mmol Zn) in a 50 mL round-bottom flask fitted with a condenser. The reaction was heated at 80 °C in an oil bath for 2 weeks. Over the initial several hours, the mixture turned off-white and thickened. The final product was collected and washed in the same way as **1**. A white powder was obtained (8.24 g, 95% yield). IR spectrum (cm^{-1}): 3415w, 2892w, 3342vw, 3277vs, 1550vs, 1388m, 1370s, 1353vs, 1040m, 969w, 880w, 795m, 760m, 753m, 635w, and 567s. Anal. Calcd for $In_{0.7}Zn_{0.3}(HCOO)_2(OH)_{0.7} \cdot 0.6H_2O$ (FW 212.74): C 11.29, H 1.85. Found: C 11.68, H 1.82.

3b was prepared in the same way as **3a** but with a starting In:Zn of 70:30 at % using 14.0 mmol In_2O_3 and 2.40 mmol zinc hydroxide carbonate. IR spectrum (cm^{-1}): 2986vw, 2915w, 2892vw, 1633m, 1572s, 1550vs, 1402m, 1387s, 1363vs, 1329s, 1152w, and 792vs. Anal. Calcd for $In_{0.74}Zn_{0.26}(HCOO)_{2.74}$ (FW 225.32): C 14.61, H 1.23. Found: C 14.81, H 1.34.

Synthesis of $In_xZn_{(1-x)}(HCOO)_{(2+x-y)}(OH)_y \cdot zH_2O$ with H_2O (4). Prepared in the same way as **3a** but using a HCOOH−deionized water (1:1 vol) addition and a reaction period of 1 week. 2−3 mm long crystals were observed growing out of the precipitate. The white precipitate (**4a**) (6.50 g, 75% yield) and crystals (**4b**) (71.7 mg) were separated and washed. IR spectrum of **4a** (cm^{-1}): 3415m, 3355w, 3272w, 2978vw, 2908w, 1604m,

(27) Kageyama, H.; Khomskii, D. I.; Levitin, R. Z.; Vasil'ev, A. N. *Phys. Rev. B* **2003**, *67*(22), 224422.
(28) Post, M. L.; Trotter, J. *Acta Crystallogr.* **1974**, *B30*, 1880.
(29) Stoilova, D. *J. Mol. Struct.* **2006**, *798*, 141.
(30) Viertelhaus, M.; Anson, C. E.; Powell, A. K. *Z. Anorg. Allg. Chem.* **2005**, *631*(12), 2365.
(31) Dollimore, D.; Tonge, K. H. *J. Inorg. Nucl. Chem.* **1969**, *29*, 621.
(32) Sapina, F.; Burgos, M.; Escriva, E.; Folgado, J. V.; Marcos, D.; Beltran, A.; Beltran, D. *Inorg. Chem.* **2002**, *32*(20), 4337.
(33) Viertelhaus, M.; Henke, H.; Anson, C. E.; Powell, A. K. *Eur. J. Inorg. Chem.* **2003**, *2003*(12), 2283.
(34) Stoilova, D.; Baggio, R.; Garland, M. T.; Marinova, D. *Vib. Spectrosc.* **2007**, *43*(2), 387.
(35) Vassileva, V. Z. *Croat. Chem. Acta* **2005**, *78*(2), 295.
(36) Su, J.; Wang, Y.; Yang, S.; Li, G.; Liao, F.; Lin, J. *Inorg. Chem.* **2007**, *46*, 8403.

Table 1. Comparison of Cation Ratio for Reagent Mixture and Final Product

	cation ratio (at % In)		
	starting material	product by ICP-AES	product by XRF
3a (**1**)	65	69.8 ± 0.6	71.4 ± 2.1
3a (**2**)	65	66.6 ± 1.2	73.1 ± 6.3
3b	70	73.9 ± 0.7	74.1 ± 1.9
4a	65	86.1 ± 0.5	82.7 ± 4.5
4b	65	1.05 ± 0.05	1.55 ± 0.25

1543vs, 1396w, 1383m, 1352vs, 1036s, 879w, 838w, 796s, 767s, 634s, and 566s. Anal. Calcd for $In_{0.83}Zn_{0.17}(HCOO)_2(OH)_{0.83}\cdot 0.34H_2O$: C 11.09, H 1.63. Found: C 11.06, H 1.68. IR spectrum of **4b** (cm^{-1}): 3346m, 3268m, 3170m, 2984vw, 2900w, 1667w, 1560vs, 1396m, 1374s, 1352vs, 878w, 836w, 761m, 722m, and 565m. Anal. Calcd for $Zn_{0.99}In_{0.01}(HCOO)_2\cdot 2H_2O$: C 12.55, H 3.15. Found: C 12.62, H 3.06.

Results and Discussion

Synthesis. The series of compounds were synthesized by neutralization. The bubbling observed during the synthesis of **1** using $[ZnCO_3]_2\cdot[Zn(OH)_2]_3$ was expected, as CO_2 and H_2O are byproducts of the neutralization with heating. Bubbling stopped shortly after the stoichiometric amount of HCOOH was added. Similar initial bubbling was observed in the case of the mixed cation reactions (**3** and **4**), which also used $[ZnCO_3]_2\cdot[Zn(OH)_2]_3$, suggesting the zinc formate establishes itself in solution much earlier than the indium formate. Its presence appeared to accelerate the indium formate formation, as evident when comparing the consistency of the indium formate synthesis to the mixed cation synthesis. While reaction mixture **2** showed no visible difference (a yellow suspension of In_2O_3) after 5 h, reaction mixtures for **3** and **4** had significantly thickened. Reaction **4** was carried out with an equal volume of HCOOH and water, which further altered the process because of solubility differences, as noted by the presence of crystals (**4b**) growing out of the precipitate (**4a**) upon cooling. All products were washed with THF instead of water to remove residual HCOOH without washing away product. **1** was especially soluble in water.

Cation Composition. As the conductivity and phases of the In−Zn-oxide system are dependent on the cation ratio, knowing the ratio in the precursors was critical.[6,7] The compounds were synthesized with a target of 65−80 cation% In. Table 1 compares the cation ratio of the reagents to the measured ratio of the products. Reported uncertainties are the standard deviations of five replicates for ICP-AES and six spots per sample for XRF, with **3a** (**1**) and **3a** (**2**) denoting two separate synthesis attempts. The XRF results are in agreement with ICP-AES given their uncertainties.

The cation composition results reveal several important factors. First, the indium fraction of the products was higher than the mixed fraction in the reagents. The preferential solubility of zinc formate resulted in the zinc being retained in solution and not incorporated into the product precipitate, hence the product being zinc deficient. Therefore, it was hard to guarantee a final composition by simply mixing a desired starting stoichiometry. The effect was enhanced in the case of reaction **4**. Given the high solubility of **1** in water, it was not surprising that the precipitate (**4a**) was more In-rich with 86 cation% In and that $Zn(HCOO)_2\cdot 2H_2O$ crystals grew out of the solution upon cooling (**4b**).

Second, not only was the composition difficult to reproduce between batches, but it also varied within a batch. XRF provided a non-destructive method to randomly sample each powder within a ~800 μm spot size to examine compositional uniformity. Compositional variation was 2.6−5.4% (relative percent) over different spots within a batch. This is significantly larger than the instrumental precision of 0.9%. For example, the concentration of **3a** (**1**) at nominally 71 cation% In actually varied by ±2.1 absolute cation% (a 2.9% relative variation) depending on what portion of the powder sample was analyzed. The non-uniformity can be attributed to the reaction involving a suspended solid phase as opposed to a homogeneous solution. Furthermore, the collected material was a mixture of two separate compounds. The effect was most pronounced in the case of **3a** (**2**), where difficultly was encountered stirring the reaction mixture, resulting in a variation of 8.6%.

Overall, the difficulties in tailoring the final cation composition and maintaining compositional uniformity bring into question the practicality of co-synthesized In−Zn formates as potential single-source precursors for TCOs. Investigations into more reproducible synthetic routes are ongoing. While such control is desirable for large-scale production consistency, a single composition is not required for a-IZO phase formation from a materials perspective. Taylor et al. has shown that the material is amorphous over a large composition region from 55 to 84 cation% In when sputtered. Furthermore, maximum conductivity can be achieved in this region by not only tuning the cation ratio but also by adjusting oxygen content in the sputter gas.[7,8] This behavior in the sputtered material suggests that a variation of cation composition in a solution processed material because of the precursor could be compensated for by controlling oxygen content in the film during deposition or with a post-anneal treatment to achieve the desired electronic and optical properties.

IR. Figure 1 shows the FTIR absorbance spectra of the compounds. Peak listings are provided in the Experimental Section. There were two principle diagnostic regions in the IR spectra: the O−H stretch region (3600−3000 cm^{-1}) and the formate bands. The former provided information about the hydrate structure and OH-substitution. Samples were dried in-vacuo for 36 h to minimize interference from adsorbed water. The latter was distinguished by characteristic formate vibrational modes: C−H stretching (~2900 cm^{-1}), asymmetric O−C−O stretching (~1550 cm^{-1}), symmetric O−C−O stretching (~1370 cm^{-1}), and symmetric O−C−O bending (~790 cm^{-1}).[37,38]

The spectrum of **1** was typical of metal formate dihydrates.[29,39] Conversely, **2** showed no O−H bands, which is consistent with the compound being anhydrous. The mixed cation formate compounds exhibited various degrees of hydration and OH-substitution. **3a** showed

(37) Heyns, A. M. *J. Mol. Struct.* **1985**, *127*, 9.
(38) Moura, M. R.; Paschoal, C. W. A.; Ayala, A. P.; Guedes, I.; Leyva, A. G.; Polla, G.; Vega, D.; Perazzo, P. K. *J. Raman Spectrosc.* **2002**, *33*, 273.
(39) Heyns, A. M. *J. Mol. Struct.* **1985**, *127*, 217.

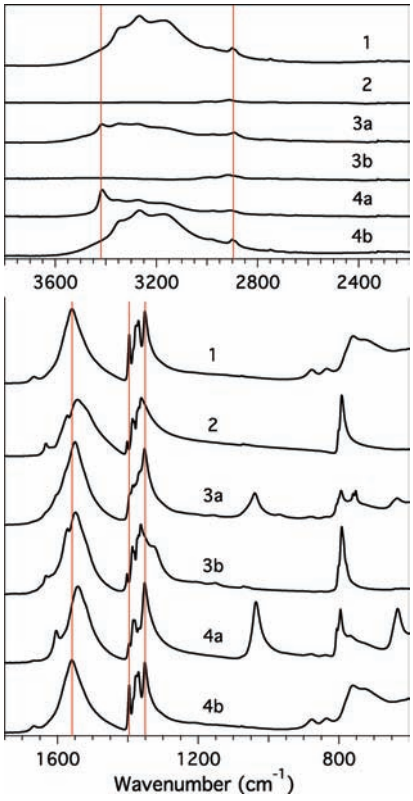

Figure 1. FTIR absorbance spectra of **1**, **2**, **3a**, **3b**, **4a**, and **4b**. Vertical lines provided as visual aid.

weak stretching peaks for both hydration and OH-substitution for formate anions in the structure, the latter being indicated by a distinct peak at higher frequency ($\sim$3415 cm^{-1}) and bending at $\sim$1040 cm^{-1}. Su et al. noted similar peaks for $In_2(HCOO)_5(OH)$ and $In(HCOO)_2(OH)$.[36] Interestingly, **3b** was anhydrous and did not show any O−H peaks for water nor OH-substitution even though it was synthesized similarly to **3a**. The cause for the differences in hydration between the products is now under investigation but was possibly due to a lack of experimental control on water content in the reaction mixture, either as a neutralization product or from the solvent. While a small fraction of **1** was detected in **4a**, the remaining vibrational pattern most closely matches that of $In(HCOO)_2(OH)$.[36] The spectrum of **4b** matched **1**.

Structure. XRD powder patterns of the compounds are provided in Figure 2 and further aided in the identification of the mixtures. Powder patterns of $In(HCOO)_3$ and $In(HCOO)_2(OH)$ are included as reference. They were simulated using CrystalDiffract 5.1 from the crystallographic information files (CIF) provided in the Supporting Information of Su et al.[36] The XRD pattern of **2** was in agreement with hexagonal $In(HCOO)_3$. **4a** strongly matched with the peak positions of tetragonal $In(HCOO)_2(OH)$. Interestingly, the pattern for **3a** was consistent with **2** and not **4a**. This was unexpected given that IR results showed **3a** to be OH-substituted, and elemental analysis was consistent with a $\sim$1:1 In:OH ratio. Thus, the powder diffraction results suggest that the OH-substituted In formate in **3a** adopted the hexagonal $In(HCOO)_3$ rather than tetragonal $In(HCOO)_2(OH)$ crystal structure. The exact nature of OH incorporation could not be determined from the given data,

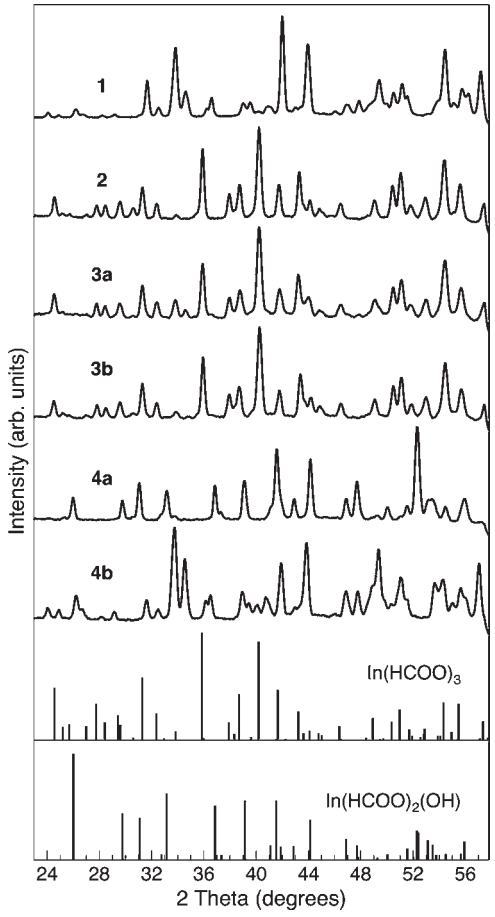

Figure 2. XRD powder patterns of **1**, **2**, **3a**, **3b**, **4a**, and ground crystals of **4b**. Simulated patterns of $In(HCOO)_3$ and $In(HCOO)_2(OH)$ are included as reference.

and a suitable sample for single crystal diffraction was not obtained.

It should be noted that it was difficult to detect peaks from $Zn(HCOO)_2\cdot 2H_2O$ in the mixed formates because of the small fraction of zinc material present. The only distinguishable peak for $Zn(HCOO)_2\cdot 2H_2O$ occurred at 34.6° 2θ in **3a** and 33.8° 2θ in **4a**. XRD results of the In−Zn formate compounds **3a** and **4a** suggest they were not solid solutions but instead mixtures of $Zn(HCOO)_2\cdot 2H_2O$ and OH-substituted In formate. The XRD pattern of the ground crystals of **4b** was consistent with $Zn(HCOO)_2\cdot 2H_2O$ (**1**), with a slight variation in relative peak intensity because of texturing from the fine crystalline nature of the powder.

The XRD pattern for **3b** was very similar to **2**, which is consistent with the IR results for a mixture containing mostly $In(HCOO)_3$. The XRD data was inconclusive about the nature of Zn in **3b**, although the IR results clearly indicate that it was not in its hydrated form. The thermal decomposition data (presented in the following section) suggested a mixture of anhydrous $Zn(HCOO)_2$ and $In(HCOO)_3$. A list of compounds identified in the products is summarized in Table 2.

Thermal Analysis. The thermal analysis curves of the compounds under N_2 and air atmospheres are shown in Figures 3 and 4, respectively. The curves progress in order of increasing indium content from zinc formate dihydrate (**1**) to indium−zinc formate (**3a**, **3b**, **4a**) to indium formate

Table 2. List of Compounds Identified in Products

	compounds identified
1	$Zn(HCOO)_2 \cdot 2H_2O$
2	$In(HCOO)_3$ (*hex*)[a]
3a	$Zn(HCOO)_2 \cdot 2H_2O + In(HCOO)_2(OH)$ (*hex*)[a]
3b	$Zn(HCOO)_2 + In(HCOO)_3$ (*hex*)[a]
4a	$Zn(HCOO)_2 \cdot 2H_2O + In(HCOO)_2(OH)$ (*tet*)[b]
4b	$Zn(HCOO)_2 \cdot 2H_2O$

[a] Hexagonal crystal structure (*hex*). [b] Tetragonal crystal structure (*tet*).

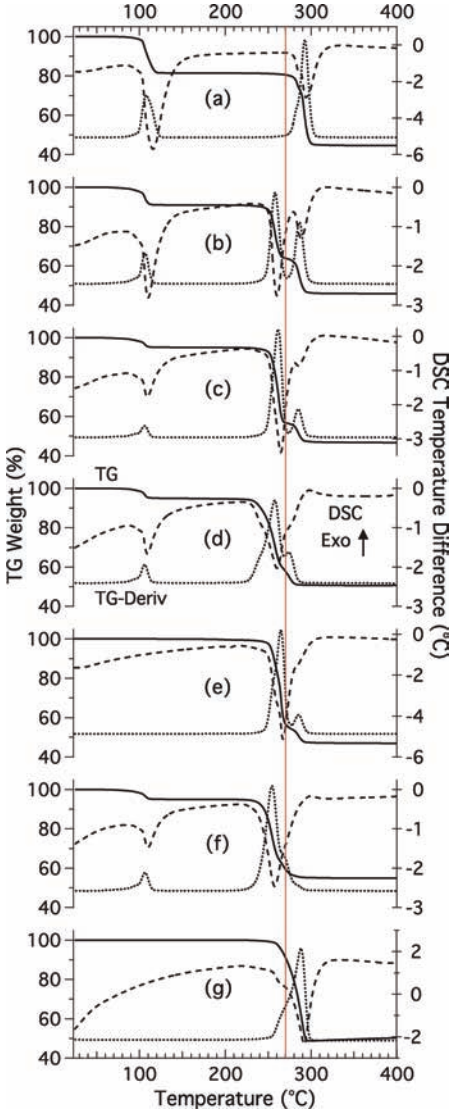

Figure 3. TG (solid) and DSC (dashed) curves of **1** (a), mixed powders of **1** and **2** with 50 cation% In (b) and 70 cation% In (c), **3a** (d), **3b** (e), **4a** (f) and **2** (g) performed under N_2. Curves are presented in order of increasing In content. TG-derivative (dotted) curves and a line at 270 °C are provided as a guide.

(**2**). Ground mixtures of **1** and **2** at 50 and 70 cation% In were included in the set to compare with the co-synthesized In−Zn formate. Table 3 summarizes the measured and calculated weight losses and decomposition temperatures.

Decomposition occurs by two principle transitions: dehydration, followed by decomposition of the anhydrous formate. Dehydration was observed for **1**, **3a**, **4a**, and the mixed individual formates, but not for **2** or **3b**. This is consistent with the IR results (Figure 1) that showed

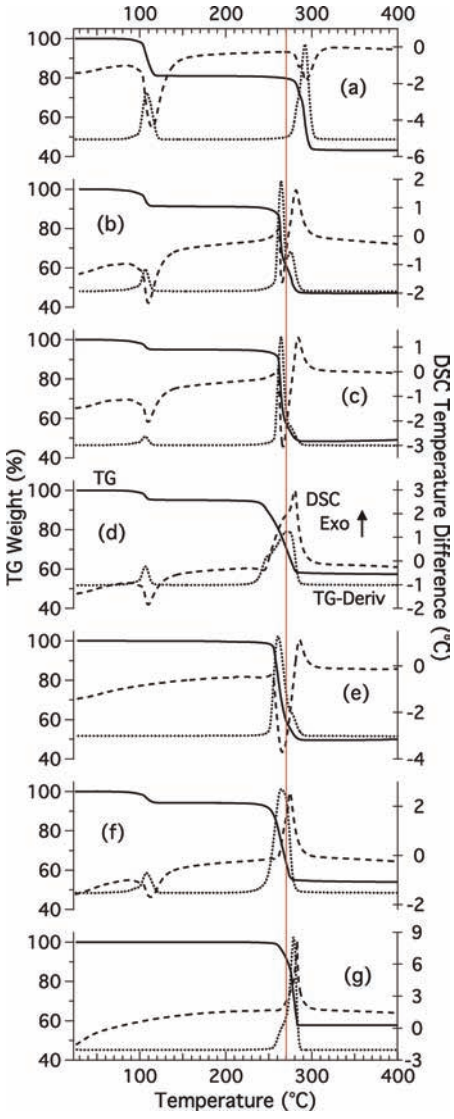

Figure 4. TG (solid) and DSC (dashed) curves of **1** (a), mixed powders of **1** and **2** with 50 cation% In (b) and 70 cation% In (c), **3a** (d), **3b** (e), **4a** (f), and **2** (g) performed under air. Curves are presented in order of increasing In content. TG-derivative (dotted) curves and a line at 270 °C are provided as a guide.

broad O−H stretching associated with a hydrated structure in all but **2** and **3b**. Similar thermal behavior was observed for dehydration with a weight loss occurring at 105−110 °C corresponding to an endothermic process. The measured weight losses were in agreement with the proposed mixture compositions.

The second decomposition stage of the formate compounds was more complex and showed distinct differences. First, there was a significant difference of ∼20 °C between the decomposition of the individual zinc and indium formates. **1** decomposed between 270 and 310 °C (peak 290 °C), but **2** decomposed at a lower temperature in air (peak 270 °C). Second, the thermal decomposition seemed to take place in two steps for the mixed formates, as indicated by the splitting of DSC peaks and a slope change in the TG curves. It is important to note that the decomposition behavior was not a superposition of the individual compounds. Instead, a shift to lower temperature by ∼5 °C was observed. This was reproducible and not an artifact of the measurement.

Table 3. TG-DSC Critical Temperatures and Weight Losses

	1	Mix 50 cation% In	Mix 70 cation% In	**3a**	**3b**	**4a**	**2**
dehydration loss (wt %)[a]	18.80 {18.82}	8.18 {8.16}	4.57 {4.65}	5.07 {5.08}		4.58 {2.83}	
decomposition temperature (°C)[b]	270−310 [290]	240−300 [258] [285]	240−300 [261] [285]	230−290 [258] [274]	240−300 [265] [285]	230−290 [254] [268]	260−300 [288] (N_2) [270] (air)
decomposition loss (wt %)[c]	55.48 (N_2) 56.68 (air) < 57.48 >	53.60 (N_2) 52.20 (air) < 50.96 >	52.88 (N_2) 50.41 (air) < 48.36 >	49.10 (N_2) 42.43 (air) < 42.84 >	53.06 (N_2) 50.11 (air) < 45.02 >	44.63 (N_2) 42.08 (air) < 40.44 >	51.05 (N_2) 42.68 (air) < 44.44 >

[a] Calculated value for dehydration weight loss { }. [b] Decomposition peak temperatures from TG derivative curve under N_2 [ ]. [c] Calculated value assuming ZnO and/or In_2O_3 products < >.

The progression of the two decomposition steps with temperature and composition is most evident upon examination of the TG derivative curves (Figure 3). The mixtures of **1** and **2** both showed weight losses between 240 and 300 °C with peak splitting at ∼258 and 285 °C. The decomposition step temperatures were independent of the cation% In.

While **3a** also exhibited peak splitting, it decomposed at an even lower temperature (230−290 °C) with peak splitting at 258 and 274 °C. Interestingly, the second peak for the co-synthesized formate occurred at a significantly lower temperature (∼10 °C) than the mixed individual formates with the same cation composition. Conversely, **3b** showed splitting similar to the mixed individual formates. This was not surprising given that the mixed individual formates were anhydrous after 110 °C. Both **3b** and the mixture were effectively $Zn(HCOO)_2$ and $In(HCOO)_3$ before the last decomposition stage. **4a** decomposed at slightly lower temperature than **3a**, peaking at 254 and 268 °C. Thermal analysis results for **4a** showed inconsistent weight losses to the degree that an accurate formula determination could not be carried out, but elemental analysis, IR, and XRD all support it being a mixture of $Zn(HCOO)_2 \cdot 2H_2O$ and $In(HCOO)_2(OH)$. In general, it was observed that a mixture of In and Zn formates reduced the decomposition temperature and that OH-substitution reduced the temperature of the second step.

We concluded that the shift to lower decomposition temperature was due to a synergistic effect between the In and Zn species. The results suggest the initial decomposition of the indium formate was assisting the decomposition of its zinc counterpart. The initial decomposition step may provide sufficient local energy to heat the zinc formate higher than the applied temperature during the analysis, thus lowering the required temperature of the second step. Such energetics are apparent when contrasting the DSC results measured under N_2 (Figure 3) and air (Figure 4). In the case of **2**, the decomposition process was endothermic under N_2 but exothermic under the air environment. This difference was attributed to atmosphere dependent reactions, with the more oxidizing atmosphere favoring formation of In_2O_3 over In metal (discussed further later). In fact, the gradual and then sudden steepness in the TG slope (almost vertical) observed under air is indicative of a highly exothermic process in which the sample heats faster than the applied heating rate. As the zinc compound exhibited only oxide formation, no change in DSC behavior was observed under different atmospheres. In the case of the mixed individual formates, the two decomposition steps were both endothermic under N_2. However, the process exhibited an endothermic to exothermic transition under air.

The energetics of **3a** and **4a** are the most revealing. The decomposition was endothermic under N_2 but appeared solely exothermic under air. Increasing the heating rate from 10 °C/min to 20 °C/min under air resulted in a DSC curve change, displaying an endotherm transitioning to an exotherm similar to that of the mixed powders. The change could be due to the reaction kinetics. With a faster heating rate, the compound may reach the required temperature and decompose (endothermic reduction) faster than oxygen can diffuse in for reaction (exothermic oxidation). The previously noted lower decomposition temperature and above-mentioned different DSC behavior of **3a** and **4a** compared to the mixed powders could be the result of co-synthesis achieving finer mixing than was achieved by physically mixing the individual formates with grinding. In principle, finer mixing would allow the local energetics of indium formate decomposition to more effectively influence the zinc formate. However, it is more probable that the effect was due to the presence of OH-substituents, which was unique to these two samples. This is supported by the fact that **4a**, with a larger fraction of $In(HCOO)_2(OH)$, exhibited an even greater decomposition temperature shift than **3a**. Furthermore, **3b**, which was anhydrous and not OH-substituted, showed a less pronounced shift and was very similar to the mixed individual formate powders in terms of TG and DSC behavior.

Finally, thermal analysis of the compounds revealed that reduction and oxide products form. The measured losses under N_2 were 53.60 wt % (Calcd 50.96 wt %) and 52.88 wt % (Calcd 48.36 wt %) for the 50 and 70 cation% In mixtures respectively. The measured losses were significantly larger than was expected for the decomposition into stoichiometric ZnO and In_2O_3 products. This effect was more significant under the reducing N_2 environment, especially in the case of **3a** with losses of 49.43 wt % (N_2) versus 42.43 wt % (air). The XRD powder patterns indicate that the decomposition products contain In metal, In_2O_3, and ZnO (Figure 5). A full list of XRD patterns for the TG decomposition products after heating to 600 °C under N_2 and air are provided in Figures S1 and S2 of the Supporting Information. Likewise, images of decompositions products are provided in Figure S3 of the Supporting Information. As shown in Figure 5, **3a** yielded a significant amount of In metal following decomposition after 300 °C and that it was converted to mostly oxide with longer heating up to 600 °C. Samples that favored oxidation (**3a** and **4a**) showed a more pronounced yellow color, indicative of In_2O_3, while samples that favored

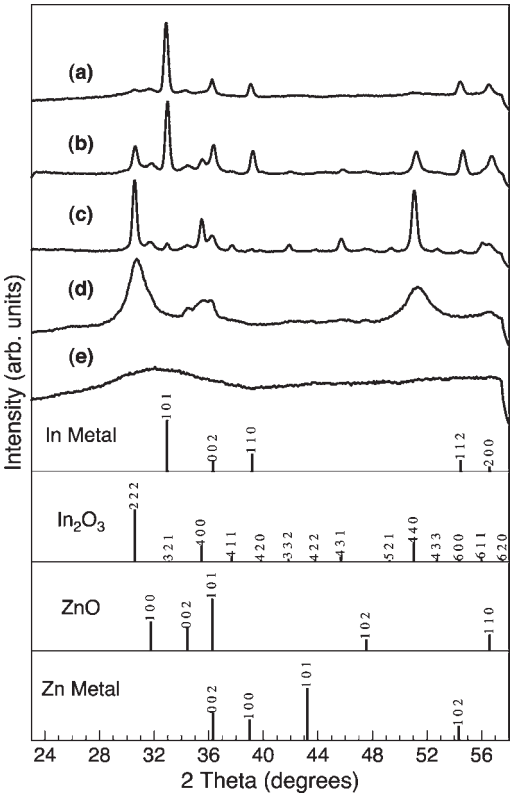

Figure 5. XRD powder patterns of resulting material from drop-cast **3a**-HCOOH solution (a), **3a** powder heated to 300 °C (b), **3a** powder heated to 600 °C (c), drop-cast **3a**-HNO_3 solution (d), and sprayed **3a**-HNO_3 film after 300 °C anneal (e). Indexed patterns of In metal, In_2O_3, Zn metal, and ZnO are included as reference.

reduction to In metal were grayer (**2** and **3b**). **3b** strongly favored reduction, producing almost entirely gray material even when the analysis was performed under air. The measured losses of 53.06 wt % (N_2) and 50.11 wt % (air) were significantly larger than was expected for the decomposition into stoichiometric oxide products (45.02 wt %).

As decomposition of formate may produce the reducing gas CO, it is not surprising that In(III) is reduced in situ to In metal. Similarly, Su et al. noted reduction products in the decomposition of $In(HCOO)_3$, $In_2(HCOO)_5(OH)$, and $In(HCOO)_2(OH)$ and that the ratio of indium metal to oxide decreased as the degree of OH-substitution increased. Furthermore, they observed CO, CO_2, and H_2O during decomposition using mass spectrometry.[36] CO can exhaust local oxygen content during decomposition, thus allowing for reduction products even in air, as was observed in the case of **3b**.

Precursor Chemistry. The reduction behavior of the formates is unique compared to the more commonly used acetate precursors. During TCO processing, films are often annealed in a reducing environment (such as forming gas) to create a non-stoichiometric oxide and thus increase electronic carrier concentration. Similarly, the presence of an inherently reducing ligand may have the advantage of chemically aiding in the introduction of carriers in lieu of or complementary to a reducing anneal.

In terms of solution processing, additives not only influence solution properties (such as wetting) but also influence the chemistry. The reducing properties of formate with indium-containing compounds even in an oxidizing environment was confirmed and exploited by drop-casting from solutions with different acid additives. Aqueous solutions of **3a** with HCOOH and HNO_3 were drop-cast onto microscope glass at 300 °C in air. Figure 5 shows typical XRD profiles of the resulting material. The addition of excess formic acid drove the reaction toward the formation of indium metal, as indicated by the relatively large In (101) peak at 32.9° 2θ. Conversely, the addition of HNO_3 (an oxidizing acid) yielded the oxide. ZnO was observed in both cases. The results suggest that In−Zn formate can be used as either an indium metal or an oxide precursor simply by taking advantage of the additive's chemistry.

Likewise, indium reduction can occur by a red-ox reaction with zinc. The reduction of In(III) to In metal, with its more positive reduction potential, is electrochemically favored in the presence of Zn metal:

$$In^{3+} + 3e^- \rightarrow In^0 \qquad E° \ -0.34 \text{ V vs SHE}$$

$$Zn^{2+} + 2e^- \rightarrow Zn^0 \qquad E° \ -0.76 \text{ V vs SHE}$$

Zhang et al. employed the process to synthesize metallic indium hollow spheres and nanotubes by reacting $InCl_3$ with Zn metal powder.[40] In the case of the In−Zn formates, if Zn metal were to form during decomposition, it would react with any In(III) present and produce In metal and ZnO, which may account for **3b** yielding a larger fraction of In metal than **2**. This is supported by the presence of In metal, In_2O_3, ZnO, but not Zn metal in the post-TG decomposition products and drop-cast material.

Sprayed IZO Films. To investigate the potential of In−Zn formates as precursors for a-IZO, films were deposited by ultrasonic spray onto microscope glass slides at 210 °C from solutions of **3a** in methanol and water with HNO_3. The method employed an ultrasonic nozzle and carrier gas to generate and direct an aerosol of precursor solution onto the substrate. It differed from other chemical vapor deposition and spray pyrolysis methods since neither vaporization of the precursor nor full decomposition of the precursor upon contact with the substrate occurred. Substrate surface temperatures were below the decomposition temperature, and annealing was required for oxide formation.

Thin films (100−200 nm) were produced with good optical transmittance (>80%) and conductivities of ~50 S/cm. The films were amorphous after thermal processing at 300−400 °C, as shown by the XRD profile in Figure 5e of a typical film after processing. The broad "hump" in the spectrum (28−39° 2θ) was indicative of amorphous material and strongly resembled the glass substrate. The ability to produce amorphous IZO by solution processing, as demonstrated here, is especially important for material applications. When sputtered, IZO is the most conductive in the amorphous state.[6,7] Additionally, its amorphous structure may make it more suitable for flexible substrates compared to other crystalline TCOs. To the best of our knowledge, this is the first reported instance of solution deposited a-IZO films. A full analysis of the structural, optical, and electronic properties of these films is the subject of a future paper.

(40) Zhang, Y.; Li, G.; Zhang, L. *Inorg. Chem. Commun.* **2004**, *7*(3), 344.

To investigate the effect of the nitric acid additive, comparative experiments were performed using solutions from only nitrate salts and from nitrate salts with formic acid as an additive. Films sprayed by these routes and processed under similar conditions exhibited extensive pinholing and were half as conductive. While this work demonstrates the potential for the formate system, additives other than HNO_3 that do not contribute a significant fraction of counterions are being explored so that a formate-only system can be studied.

Conclusions

In summary, a series of In−Zn formate mixtures exhibiting various degrees of hydration and OH-substitution were synthesized by neutralization. Individual $Zn(HCOO)_2 \cdot 2H_2O$ (**1**) and hexagonal $In(HCOO)_3$ (**2**) were prepared. Mixtures were identified as $Zn(HCOO)_2 \cdot 2H_2O$ and hexagonal $In(HCOO)_2(OH)$ with 70 cation% In (**3a**), anhydrous $Zn(HCOO)_2$ and hexagonal $In(HCOO)_3$ with 74 cation% In (**3b**), and $Zn(HCOO)_2 \cdot 2H_2O$ and tetragonal $In(HCOO)_2$-(OH) with 83 cation% In (**4a**). XRD powder diffraction results suggest that the OH-substituted **3a** adopted the hexagonal $In(HCOO)_3$ rather than tetragonal $In(HCOO)_2$-(OH) crystal structure. No evidence was found for solid solution formation in the In−Zn formate system.

It was found that the presence of both In and Zn species had a synergistic effect that resulted in an overall reduction in the decomposition temperature. OH-substitution further reduced the temperature. As a precursor, it was demonstrated that the decomposition products of In−Zn formate could be directed toward oxidation or reduction by controlling the decomposition atmosphere or with solution additives such as acids. While the focus of the paper was characterization of the precursors, it was also demonstrated that amorphous IZO films could be prepared by solution processing from In−Zn formates for TCO applications.

Acknowledgment. This work was supported by the National Center for Photovoltaics (NCPV) at the National Renewable Energy Laboratory (NREL) through U.S. Department of Energy under Contract No. DE-AC36-08GO28308. Thanks to Lynn Gedvilas and Phil Parilla at NREL for assistance with the IR and SDT measurements.

Supporting Information Available: Additional IR analysis. Characterization of **4b**. XRD powder patterns of decomposition products under air and N_2, and images of the decomposition products. Preparation and characterization of OH-substituted $In(HCOO)_{3-x}(OH)_x$ from **2**. This material is available free of charge via the Internet at http://pubs.acs.org.